Supplementary Information

Ultra-Narrowband Helical Emitter with Frontier Orbital Confinement for Stable Deep-Blue Hybrid-Tandem Organic Light-emitting Diodes

Chuanqin Cheng[#1], Minqiang Mai[#1], Chenglong Li[1], Dongdong Zhang*[1], and Lian Duan*[1,2].

[1]Key Laboratory of Organic Optoelectronics and Molecular Engineering of Ministry of Education, Department of Chemistry, Tsinghua University, Beijing, 100084, China.
[2] Laboratory of Flexible Electronics Technology, Tsinghua University, Beijing, 100084, China.
[#]These authors contribute equally to this work.

Dongdong Zhang, ddzhang@mail.tsinghua.edu.cn;
Lian Duan, duanl@mail.tsinghua.edu.cn

Table of Contents

Synthetic procedures and characterization

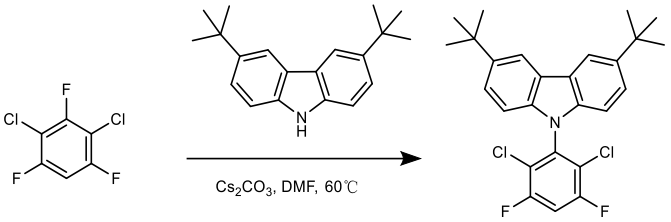

Synthesis of 3,6-di-tert-butyl-9-(2,6-dichloro-3,5-difluorophenyl)-9H-carbazole (1): Under a nitrogen atmosphere, 2,4-dichloro-1,3,5-trifluorobenzene (5 g, 24.9 mmol), 3,6-di-tert-butyl-9H-carbazole (6.9 g, 24.9 mmol), and Cs_2CO_3 (12.1 g, 37.4 mmol) were dissolved in dry N,N-dimethylformamide (100 mL). The reaction mixture was stirred at 60 ℃ for 12 hours. After cooling to room temperature,the reaction mixture was poured into water. After filtration, the crude product was purified by the silica gel column using petroleum ether as an eluent to give the pure product as a white powder (8.6 g, yielding 75%).^{1}H NMR (400 MHz, $CDCl_3$): δ 8.14-8.16 (m, 2H, Ar), 7.43-7.47 (m, 2H, Ar), 7.28 (t, J = 8.0 Hz, 1H, Ar), 6.86-6.89 (m, 2H, Ar), 1.46 (s, 18H, -CH_3). ^{13}C NMR (101 MHz, $CDCl_3$): δ 158.4, 155.8, 143.6, 137.9, 136.0, 123.9, 123.6, 116.6, 109.0, 106.0, 34.8, 32.0.

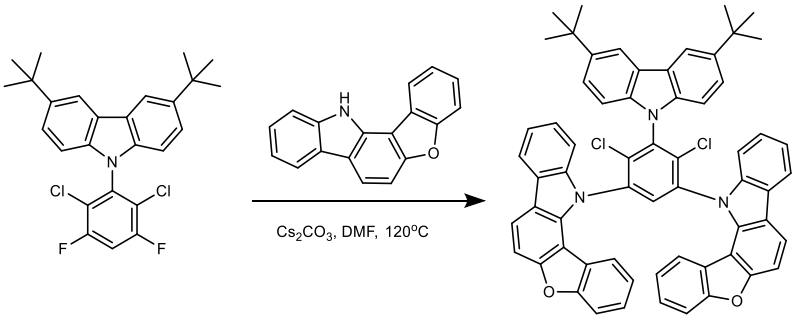

Synthesis of 12,12'-(4,6-dichloro-5-(3,6-di-tert-butyl-9H-carbazol-9-yl)-1,3-phenylene)bis(12H-benzofuro[3,2-a]carbazole) (2): Under a nitrogen atmosphere, intermediate **1** (2 g, 4.3 mmol), 12H-benzofuro[3,2-a]carbazole (2.3 g , 9.1 mmol), and Cs_2CO_3 (4.2 g, 13.0 mmol) were dissolved in dry N,N-dimethylformamide (30 mL). The reaction mixture was stirred at 120 ℃ for 24 hours. After cooling to room temperature, the reaction mixture was poured into water. After filtration, the crude product was purified by the silica gel column using petroleum ether/dichloromethane (2:1 v/v) as an eluent to give the pure product as a white powder (2.6 g, yielding 63%). ^{1}H NMR (400 MHz, $CDCl_3$): δ 8.12-8.16 (m, 4H, Ar), 8.04-8.07 (m, 4H, Ar), 7.71-7.73 (m, 2H, Ar), 7.61-7.65 (m, 2H, Ar), 7.51-7.56 (m, 4H, Ar), 7.36-7.39 (m, 2H, Ar), 7.27-7.32 (m, 3H, Ar), 7.21-7.23 (m, 2H, Ar), 7.12 (d, J = 8.0 Hz, 2H, Ar), 6.83 (d, J = 8.0

Hz, 2H, Ar), 1.43 (s, 18H, -CH_3). ^{13}C NMR (101 MHz, $CDCl_3$): δ 156.70, 156.10, 143.76, 141.27, 139.22, 138.82, 138.06, 134.07, 126.72, 125.57, 124.47, 124.08, 123.82, 122.90, 122.66, 121.92, 121.61, 119.97, 119.85, 119.77, 116.91, 112.24, 110.45, 109.11, 108.95, 105.83,34.84, 32.05.

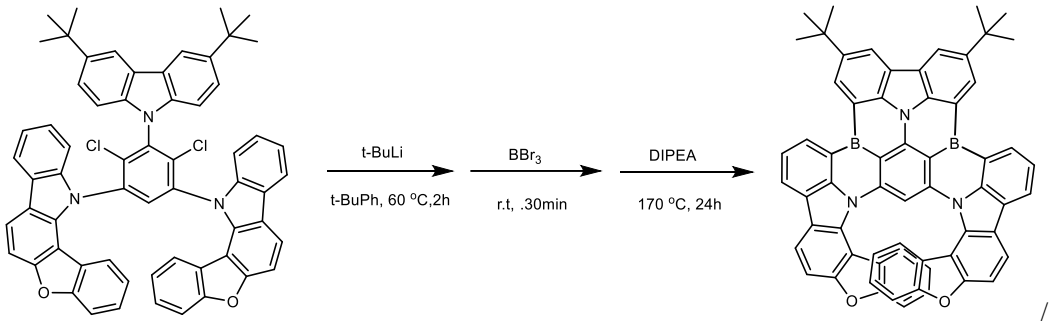

Synthesis of BD-Cz-2CzO: Under a nitrogen atmosphere, a solution of t-BuLi in pentane (7.4 mL, 1.3 M) was slowly added to a solution of intermediate **2** (2 g, 2.1 mmol) in tert-butyl benzene (50 mL) at -78 ºC. After stirring for 2 hours at 60 ºC, boron tribromide (1 mL) was added at -78 ºC, and the reaction mixture was stirred at room temperature for 2 hours. N,N-Diisopropylethylamine (2.9 mL) was added at 0 ºC, and then the reaction mixture was allowed to warm to room temperature. After stirring for 24 hours at 170 ºC, the reaction mixture was cooled to room temperature. The reaction mixture was quenched with ethanol and concentrated under reduced pressure. The crude product BD-Cz-2CzO was purified by column chromatography on silica gel (petroleum ether/dichloromethane = 2:1 v/v) and recrystallized from dichloromethane and methanol. The yield was 0.53 g, representing a 28% yield. ^{1}H NMR (400 MHz, CD_2Cl_2): δ 9.15 (s, 2H, Ar), 8.98 (d, J = 8.0 Hz, 2H, Ar), 8.78 (s, 2H, Ar), 8.41 (d, J = 8.0 Hz, 2H, Ar), 8.16 (d, J = 8.0 Hz, 2H, Ar), 7.80-7.87 (m, 3H, Ar), 7.39 (d, J = 8.0 Hz, 2H, Ar), 7.24 (d, J = 8.0 Hz, 2H, Ar), 6.75 (t, J = 8.0 Hz, 2H, Ar), 6.66 (d, J = 8.0 Hz, 2H, Ar), 5.98 (t, J = 8.0 Hz, 2H, Ar), 1.79 (s, 18H, -CH_3). The ^{13}C spectrum could not be obtained due to the poor solubility.

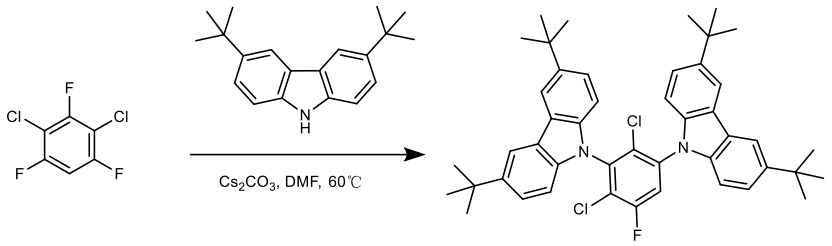

Synthesis of 9,9'-(2,4-dichloro-5-fluoro-1,3-phenylene)bis(3,6-di-tert-butyl-9H-carbazole) (3): Under a nitrogen atmosphere, 2,4-dichloro-1,3,5-trifluorobenzene (3 g, 14.9 mmol), 3,6-di-tert-butyl-9H-carbazole (8.3 g, 29.8 mmol), and Cs_2CO_3 (14.6 g, 44.7 mmol) were dissolved in dry N,N-dimethylformamide (50 mL). The reaction mixture was stirred at 60 ℃ for 12 hours. After cooling to room temperature,the reaction mixture was poured into water. After filtration, the crude product was purified by the silica gel column using petroleum ether as an eluent to give the pure product as a white powder (7.3 g, yielding 68 %). ^{1}H NMR (400 MHz, $CDCl_3$): δ 8.13-8.16 (m, 4H, Ar),7.56 (d, J = 8.0 Hz, 1H, Ar), 7.49-7.58 (m, 4H, Ar), 7.12 (d, J = 8.0 Hz, 2H, Ar), 7.01 (d, J = 8.0 Hz, 2H, Ar), 1.47 (s, 18H, -CH_3), 1.46 (s, 18H, -CH_3). ^{13}C NMR (101 MHz, $CDCl_3$): δ 143.85, 143.63, 138.85, 138.05, 124.09, 124.07, 123.84, 123.68, 118.26, 116.78, 116.67, 109.35, 109.00, 34.87, 32.09, 32.05.

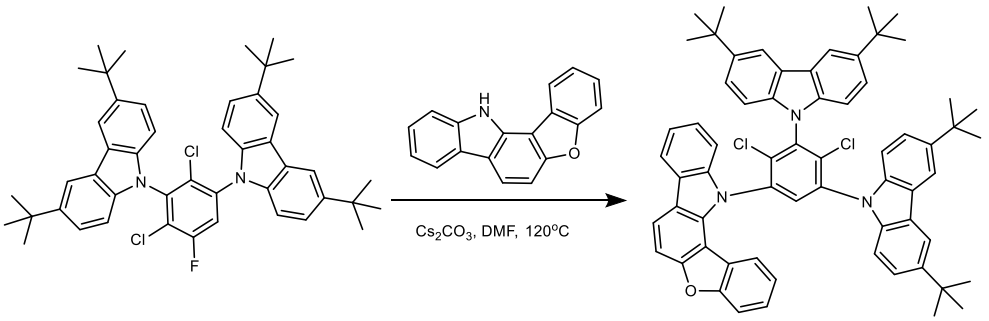

Synthesis of 12-(2,4-dichloro-3,5-bis(3,6-di-tert-butyl-9H-carbazol-9-yl)phenyl)-12H-benzofuro[3,2-a]carbazole (4): Under a nitrogen atmosphere, intermediate **3** (2 g, 2.7 mmol), 12H-benzofuro[3,2-a]carbazole (0.8 g, 3.1mmol), and Cs_2CO_3 (1.4 g, 4.2 mmol) were dissolved in dry N,N-dimethylformamide (30 mL). The reaction mixture was stirred at 120 ℃ for 24 hours. After cooling to room temperature, the reaction mixture was poured into water. After filtration, the crude product was purified by the silica gel column using petroleum ether/dichloromethane (4:1 v/v) as an eluent to give the pure product as a white powder (1.8 g, yielding 68%). ^{1}H NMR (400 MHz, $CDCl_3$): δ 8.14-8.24 (m, 4H, Ar), 8.07-8.10 (m, 2H, Ar), 8.01 (s, 1H, Ar), 7.72-7.78 (m, 1H, Ar), 7.49-7.75 (m, 6H, Ar), 7.38-7.44 (m, 2H, Ar), 7.27-7.30 (m, 2H, Ar), 7.14-7.21 (m, 3H, Ar), 7.04 (d, *J* = 8.0 Hz, 1H, Ar), 6.77 (d, *J* = 8.0 Hz, 1H, Ar), 1.50

(s, 9H, -CH_3), 1.45 (s, 18H, -CH_3), 1.41 (s, 18H, -CH_3). ^{13}C NMR (101 MHz, $CDCl_3$) : δ 156.74, 156.12, 143.90, 143.81, 143.73, 143.64, 141.07, 138.90, 138.79, 138.28, 138.09, 137.92, 137.59, 137.12, 136.95, 133.20, 126.72, 125.73, 124.39, 124.20, 124.10, 124.01, 123.92, 123.85, 123.70, 122.95, 122.76, 121.83, 121.52, 119.88, 119.71, 116.91, 116.71, 116.62, 112.18, 109.88, 109.26, 109.18, 108.97, 108.67, 105.65, 34.88, 34.83, 34.76, 32.07, 32.03, 32.00, 31.95.

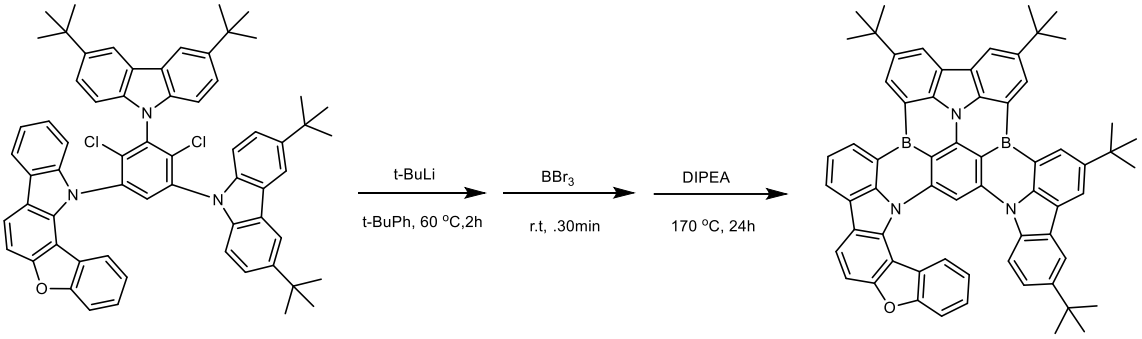

Synthesis of BD-2Cz-CzO: Under a nitrogen atmosphere, a solution of t-BuLi in pentane (5.4 mL, 1.3 M) was slowly added to a solution of intermediate **4** (1.5 g, 1.6 mmol) in tert-butyl benzene (50 mL) at -78 ºC. After stirring for 2 hours at 60 ºC, boron tribromide (0.7 mL) was added at -78 ºC, and the reaction mixture was stirred at room temperature for 2 hours. N,N-Diisopropylethylamine (2.1 mL) was added at 0 ºC, and then the reaction mixture was allowed to warm to room temperature. After stirring for 24 hours at 170 ºC, the reaction mixture was cooled to room temperature. The reaction mixture was quenched with ethanol and concentrated under reduced pressure. The crude product BD-2Cz-CzO was purified by column chromatography on silica gel (petroleum ether/dichloromethane = 3:1 v/v) and recrystallized from dichloromethane and methanol. The yield was 0.43 g, representing a 31% yield. ^{1}H NMR (400 MHz, CD_2Cl_2): δ 9.07 (m, 2H, Ar),8.54-8.60 (m, 2H, Ar), 8.43 (s, 2H, Ar), 8.25 (d, J = 8.0 Hz, 1H, Ar), 8.02-8.08 (m, 2H, Ar), 7.87-7.94 (m, 2H, Ar), 7.55 (t, J = 8.0 Hz, 1H, Ar), 7.44 (d, J = 8.0 Hz, 1H, Ar), 7.36 (d, J = 8.0 Hz, 1H, Ar), 6.90 (d, J = 4.0 Hz, 1H, Ar), 6.63-6.70 (m, 2H, Ar), 6.53-6.57 (m, 1H, Ar), 6.11 (t, J = 8.0 Hz, 1H, Ar), 1.83 (s, 18H, -CH_3), 1.80 (s, 18H, -CH_3), 1.72 (s, 18H, -CH_3), 1.52 (s, 18H, -CH_3).

Optical simulations of OLED devices

To characterize the properties of OLED device, a theoretical model based on the classical dipole and microcavity theory is utilized[1,2].

For isotropic dipole orientation, the total spectral power density K per unit normalized in-plane wave vector can be represented as below [3-7]

$$K=\mathrm{Re}\left\{\frac{u^2}{4\sqrt{1-u^2}}\left[\frac{\left(1+a_+^{\mathrm{TM}}\right)\left(1+a_-^{\mathrm{TM}}\right)}{\left(1+a^{\mathrm{TM}}\right)}+\frac{\left(1-u^2\right)}{u^2}\frac{\left(1-a_+^{\mathrm{TM}}\right)\left(1-a_-^{\mathrm{TM}}\right)}{\left(1-a^{\mathrm{TM}}\right)}+\frac{\left(1+a_+^{\mathrm{TE}}\right)\left(1+a_-^{\mathrm{TE}}\right)}{u^2\left(1-a^{\mathrm{TE}}\right)}\right]\right\} \quad (1)$$

Here $\mathrm{Re}\{\ldots\}$ denotes the real part of the complex quantity enclosed by brackets, and the normalized in-plane wave vector $u=k_\rho/k_e=\sin\theta$, where k_e stands for the total wavevector of emission layer, and k_ρ is the projection of k_e in the dipole plane. In addition, the coefficient a and $a_{+(-)}$ are defined as the following

$$a_{+(-)}^{\mathrm{TE(TM)}}=r_{+(-)}^{\mathrm{TE(TM)}}\exp\left(2jk_{z,e}z_{+(-)}\right) \quad (2)$$

$$a^{\mathrm{TE(TM)}}=r_+^{\mathrm{TE(TM)}}r_-^{\mathrm{TE(TM)}}\exp\left(2jk_{z,e}d_e\right) \quad (3)$$

In Eqs.(2)-(3), we have the wavevector $k_{z,e}=k_e\sqrt{1-u^2}=2\pi n_e\sqrt{1-u^2}/\lambda$, where λ and n_e denote the wavelength and the refractive index of emission layer, respectively. Furthermore, $z_{+(-)}$ is the distance of the dipole from the right (left) interface of the emission layer, and $r_+^{\mathrm{TE(TM)}}\left(r_-^{\mathrm{TE(TM)}}\right)$ stands for the reflection coefficient for waves traveling from the dipole layer to the right-side(left-side), and can be obtained from the below

$$r_-^{\mathrm{TE(TM)}}=-\frac{s_{12}^{-,\mathrm{TE(TM)}}}{s_{11}^{-,\mathrm{TE(TM)}}} \quad (4)$$

$$r_+^{\mathrm{TE(TM)}}=-\frac{s_{21}^{+,\mathrm{TE(TM)}}}{s_{11}^{+,\mathrm{TE(TM)}}} \quad (5)$$

Based on transfer matrix approach[8], $s^{-(+)}$ can be obtained from the 2x2 matrix defined as below:

$$S^-=I^{0/1}L^1\left(d_1\right)\ldots I^{q-1/j}L^q\left(z_e\right)=\begin{bmatrix}s_{11}^{-,\mathrm{TE(TM)} & s_{12}^{-,\mathrm{TE(TM)}}\\ s_{21}^{-,\mathrm{TE(TM)}} & s_{22}^{-,\mathrm{TE(TM)}}\end{bmatrix} \quad (6)$$

$$S^{+}=I^{q/q+1}L^{q+1}\left(d_{q+1}\right)...I^{m-1/m}L^{m}\left(d_{m}\right)I^{m/m+1}=\begin{bmatrix}s_{11}^{+,\mathrm{TE(TM)}} & s_{12}^{+,\mathrm{TE(TM)}}\\ s_{21}^{+,\mathrm{TE(TM)}} & s_{22}^{+,\mathrm{TE(TM)}}\end{bmatrix} \quad (7)$$

The dipole is located at the q-th layer. The interface matrix (I) and the layer matrix (L) in Eqs(6)-(7) are defined as the follwing

$$I^{j/j+1}=\frac{1}{t_{j/(j+1)}^{\mathrm{TE(TM)}}}\begin{bmatrix}1 & r_{j/(j+1)}^{\mathrm{TE(TM)}}\\ r_{j/(j+1)}^{\mathrm{TE(TM)}} & 1\end{bmatrix} \quad (8)$$

$$L^{j}=\begin{bmatrix}\exp\left(-ik_{z,j}d_{j}\right) & 0\\ 0 & \exp\left(ik_{z,j}d_{j}\right)\end{bmatrix} \quad (9)$$

In Eq.(9), we have the wavevector $k_{z,e}=k_e\sqrt{1-u^2}=2\pi n_e\sqrt{1-u^2}/\lambda$. The coefficient $r_{j/(j+1)}^{\mathrm{TE(TM)}}$ and $t_{j/(j+1)}^{\mathrm{TE(TM)}}$ of Eq.(8) refer to the complex Fresnel reflection and transmission coefficients at the interface from the j-th to (j+1)-th layers. Theses coefficients are expressed as below

$$r_{j/(j+1)}^{\mathrm{TE}}=\frac{\sqrt{\tilde{n}_j^2-n_e^2u^2}-\sqrt{\tilde{n}_{j+1}^2-n_e^2u^2}}{\sqrt{\tilde{n}_j^2-n_e^2u^2}+\sqrt{\tilde{n}_{j+1}^2-n_e^2u^2}}\quad,\quad r_{j/(j+1)}^{\mathrm{TM}}=\frac{\sqrt{\tilde{n}_j^2-n_e^2u^2}/\tilde{n}_j^2-\sqrt{\tilde{n}_{j+1}^2-n_e^2u^2}/\tilde{n}_{j+1}^2}{\sqrt{\tilde{n}_j^2-n_e^2u^2}/\tilde{n}_j^2+\sqrt{\tilde{n}_{j+1}^2-n_e^2u^2}/\tilde{n}_{j+1}^2}$$

$$t_{j/(j+1)}^{\mathrm{TE}}=\frac{2\sqrt{\tilde{n}_j^2-n_e^2u^2}}{\sqrt{\tilde{n}_j^2-n_e^2u^2}+\sqrt{\tilde{n}_{j+1}^2-n_e^2u^2}}\quad,$$

$$t_{j/(j+1)}^{\mathrm{TM}}=\frac{2\sqrt{\tilde{n}_j^2-n_e^2u^2}}{\tilde{n}_{j+1}\sqrt{\tilde{n}_j^2-n_e^2u^2}/\tilde{n}_j+\tilde{n}_j\sqrt{\tilde{n}_{j+1}^2-n_e^2u^2}/\tilde{n}_{j+1}}$$

Here $\tilde{n}_j$ denotes the complex refractive index of the j-th layer.

The total radiated power F at the dipole location, can be obtained by integrating K with respective to u^2 as expressed below

$$F=\int_0^\infty Kdu^2=2\int_0^\infty uKdu \quad (10)$$

where the uK is the power dissipation spectra that can be utilized to calculate the mode contributions according to different region of u. The regions $0\le u\le n_0/n_e$, $n_0/n_e\le u\le n_s/n_e$, $n_s/n_e\le u\le 1$, and $u>1$ are corresponding to air, substrate, waveguide, and surface plasmonic polariton modes, respectively [4].

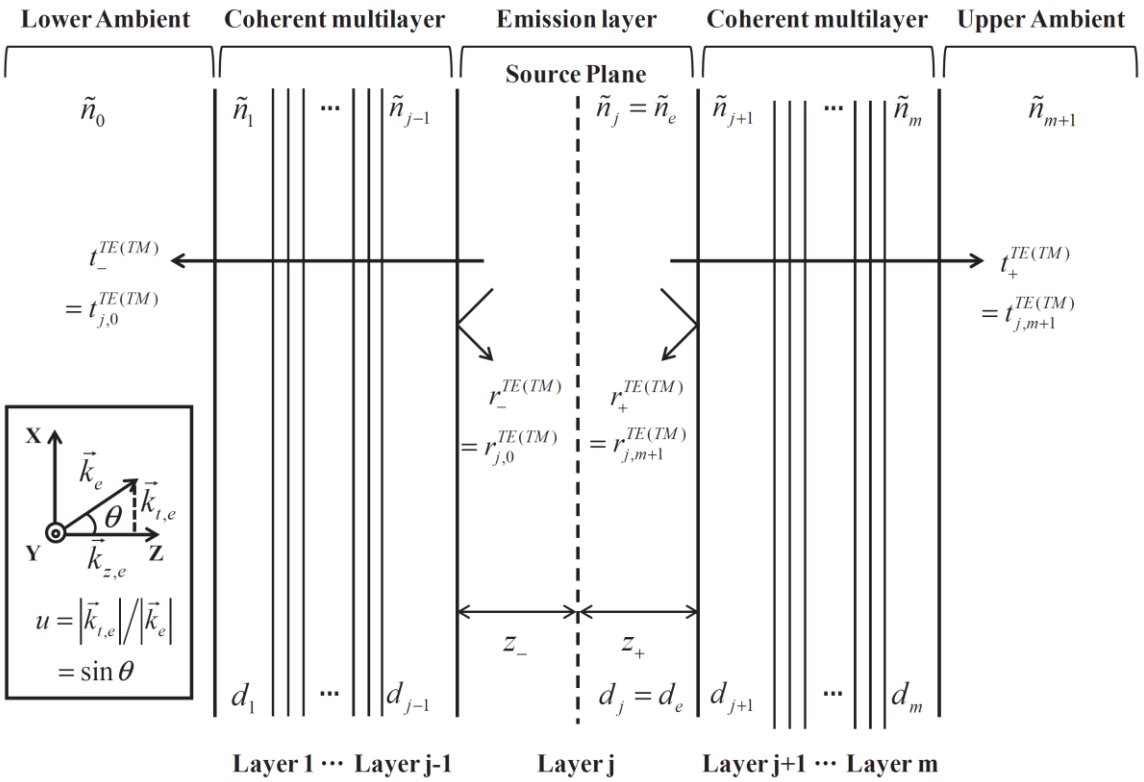

Scheme.1. Schematic diagram of the OLED made up of coherent multilayers enclosed with semi-infinite ambient layers.[5]

Supplymentary Figures and Tables

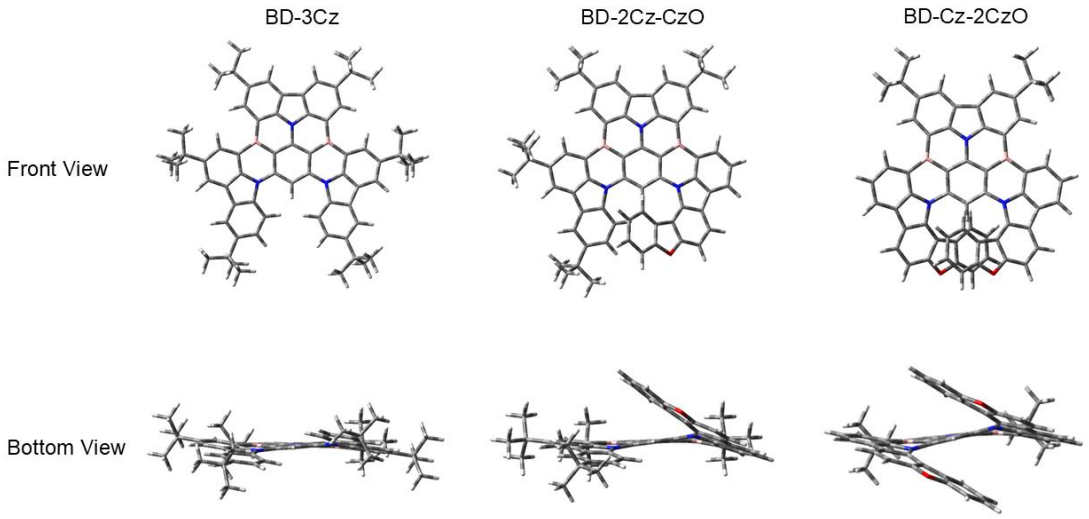

Supplementary Fig. 1 Optimized structures of BD-3Cz, BD-2Cz-CzO and BD-Cz-2CzO.

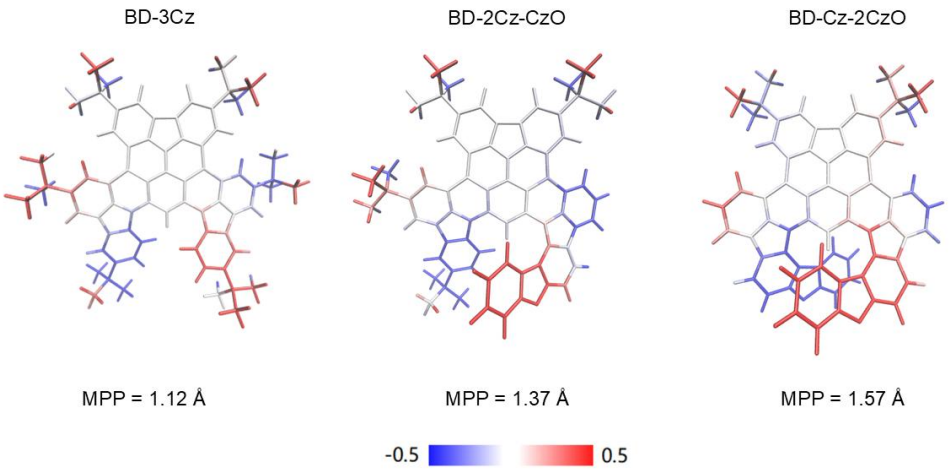

Supplementary Fig. 2 The molecular planarity parameter (MPP) values of BD-3Cz, BD-2Cz-CzO and BD-Cz-2CzO.

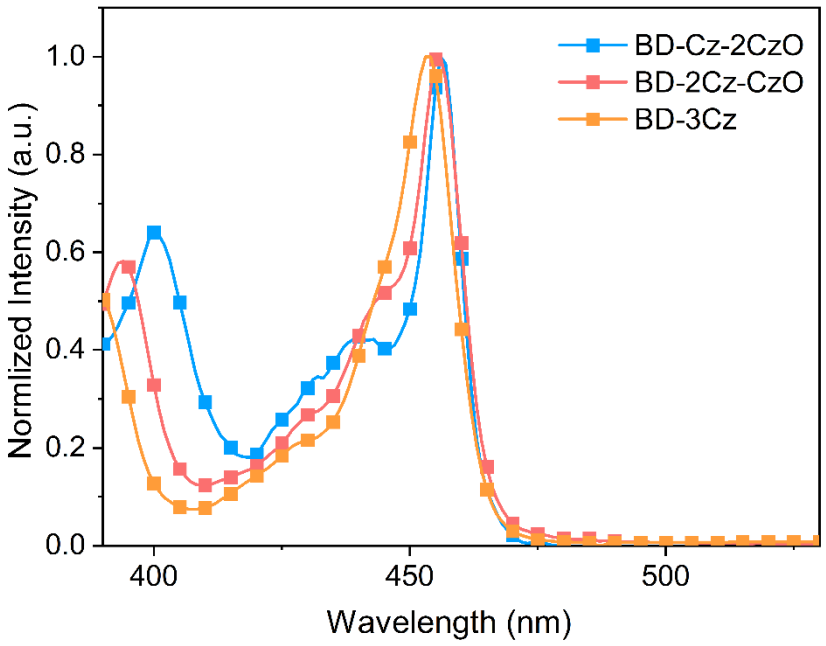

Supplementary Fig. 3 UV–vis absorption spectra at room temperature of BD-3Cz, BD-2Cz-CzO, and BD-Cz-2CzO in dilute toluene solution.

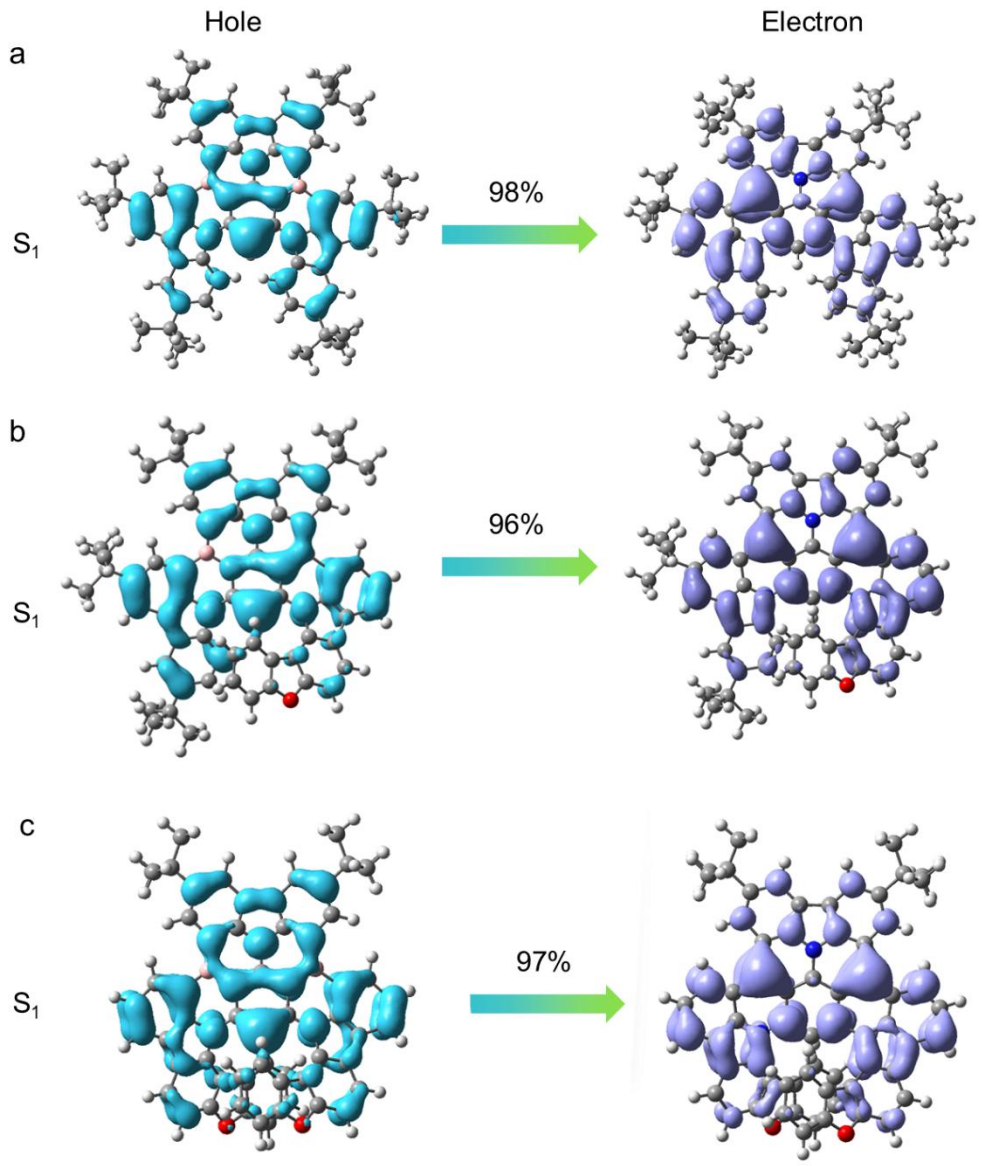

Supplementary Fig. 4 Hole-electron analysis describing the excitation characters of the S_1 in BD-3Cz (a), BD-2Cz-CzO (b), and BD-Cz-2CzO (c).

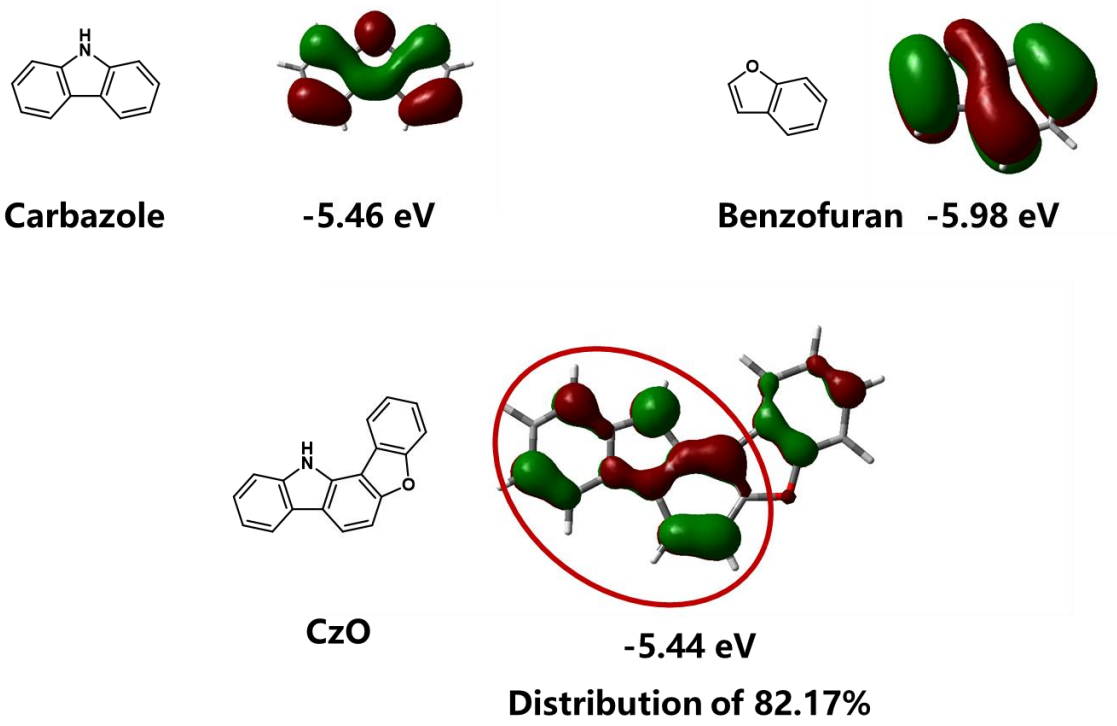

Supplementary Fig. 5 Frontier molecular orbital distributions of carbazole, benzofuran and CzO.

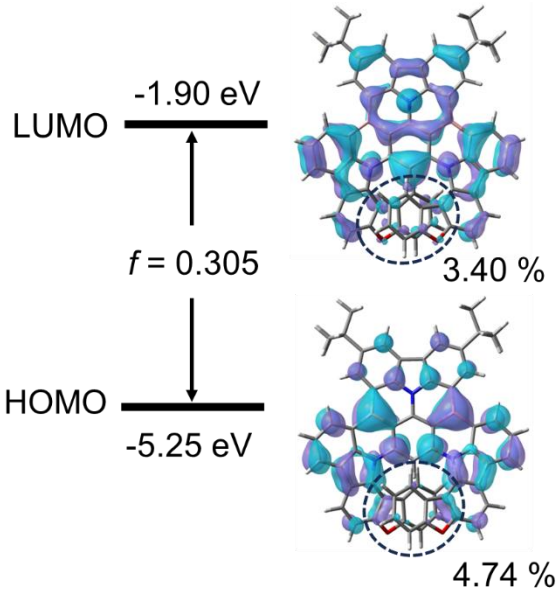

Supplementary Fig. 6 The contribution of benzofuran part to the HOMO and LUMO distribution of the whole molecule of BD-Cz-2CzO.

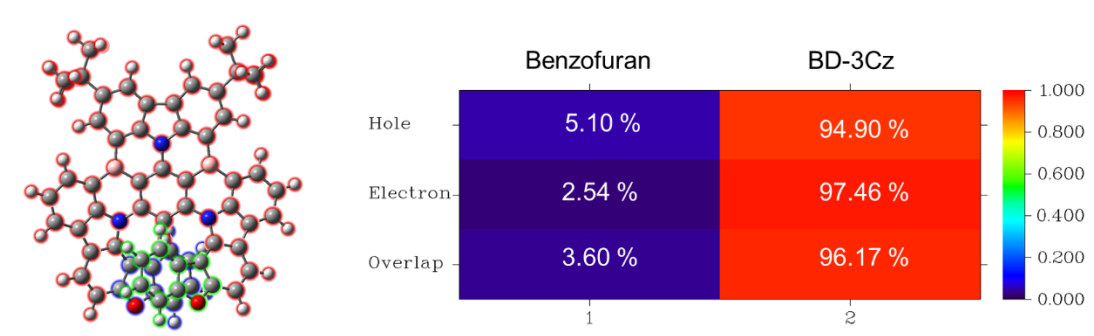

Supplementary Fig. 7 The heat map of the contribution of the benzofuran segment to the distribution of holes and electrons during the charge transfer excitation process.

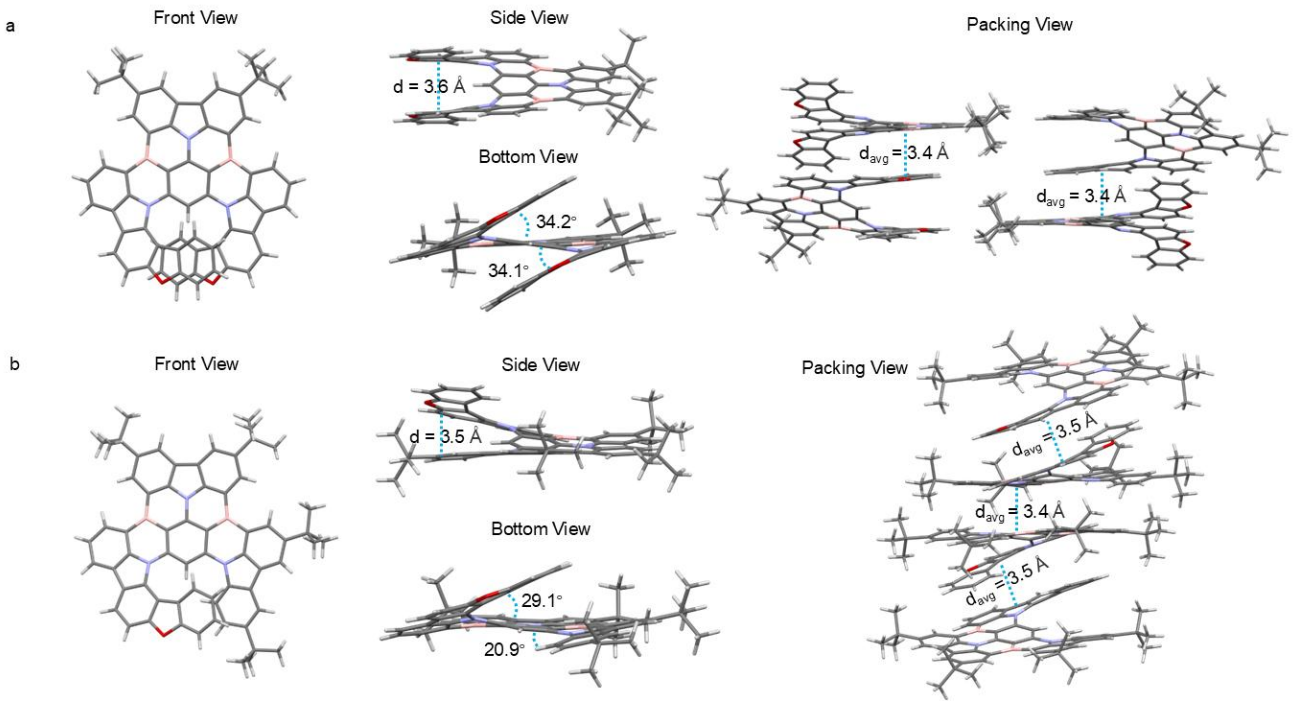

Supplementary Fig. 8 Single-crystal X-ray diffraction molecular structures of BD-Cz-2CzO (a) and BD-2Cz-CzO (b).

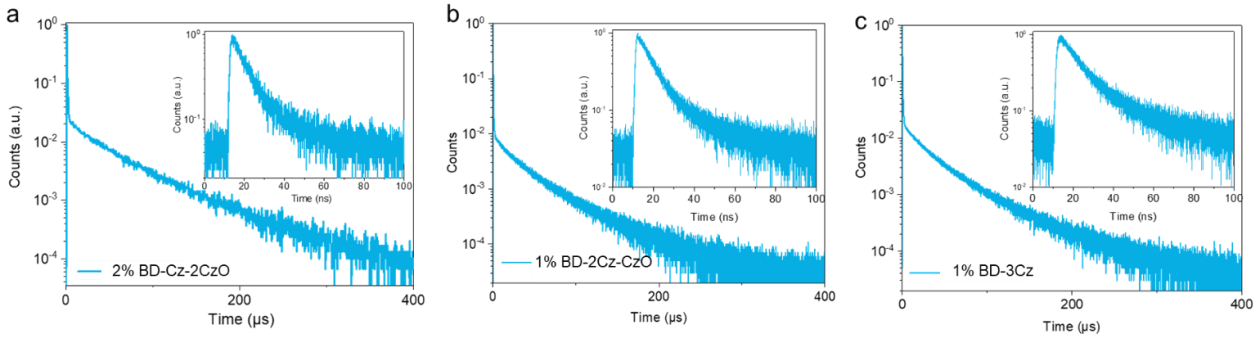

Supplementary Fig. 9 Transient PL decay curves of BD-Cz-2CzO (a), BD-2Cz-CzO (b), and BD-3Cz (c) doped films.

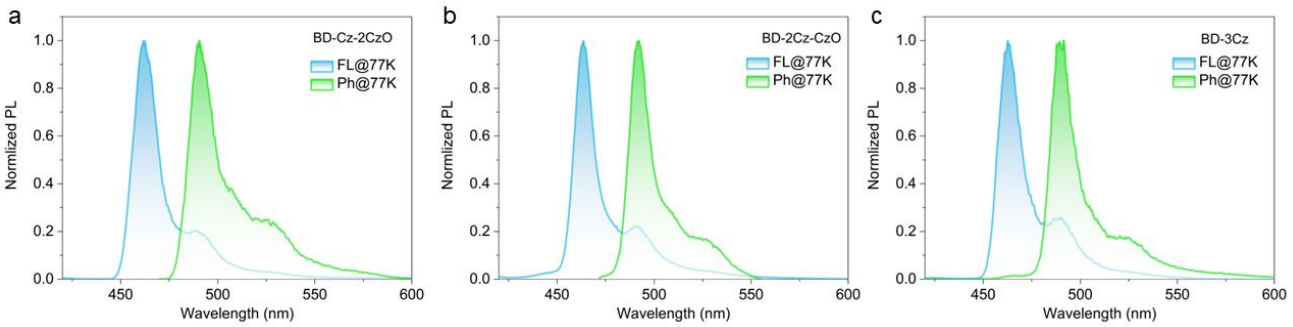

Supplementary Fig. 10 Fluorescence (77 K) and phosphorescent (77 K) spectra of BD-Cz-2CzO (a), BD-2Cz-CzO (b), and BD-3Cz (c) in dilute toluene solution.

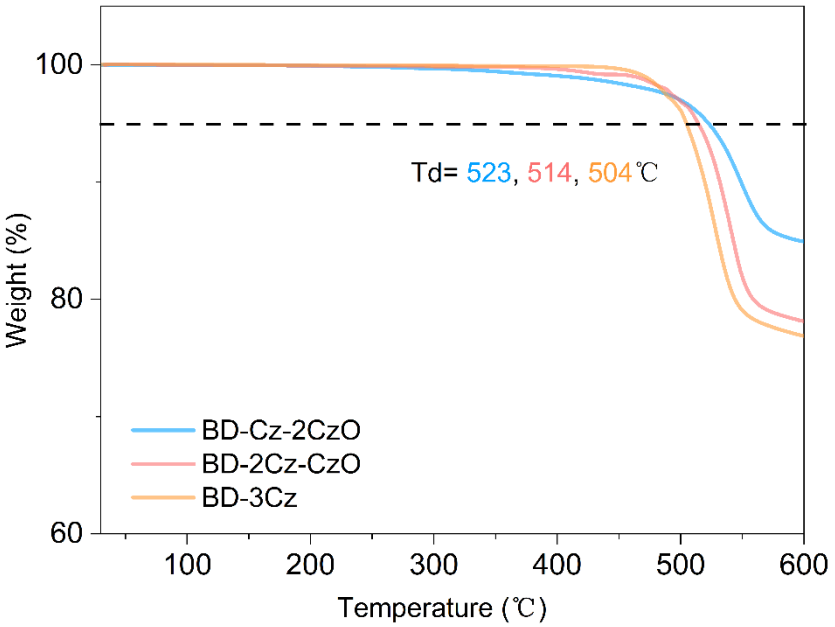

Supplementary Fig. 11 TGA thermogram of BD-Cz-2CzO at a heating rate of 10 ℃ min^{-1}.

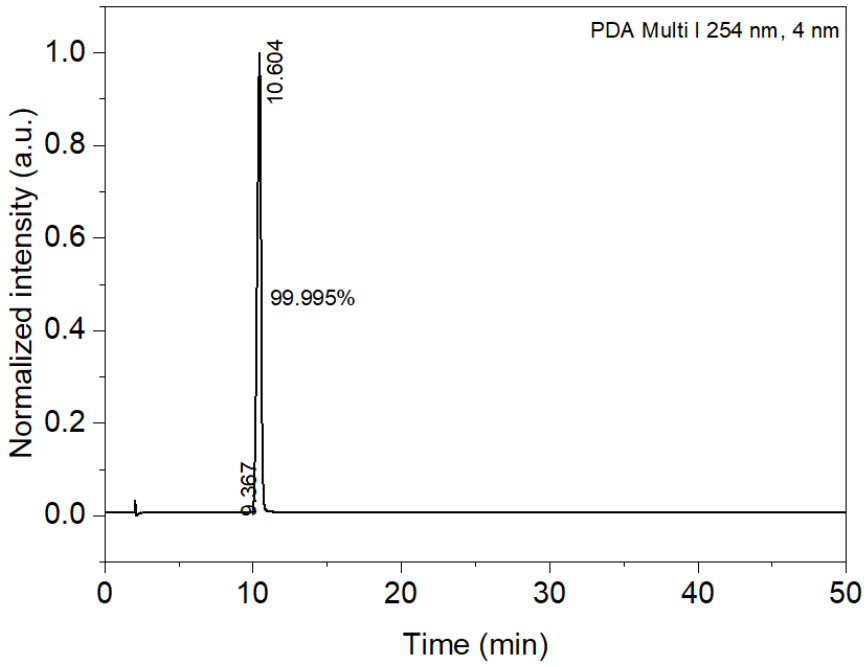

Supplementary Fig. 12 High performance liquid chromatography (HPLC) spectrum of BD-Cz-2CzO after 240 hours of continuous heating at 360 °C.

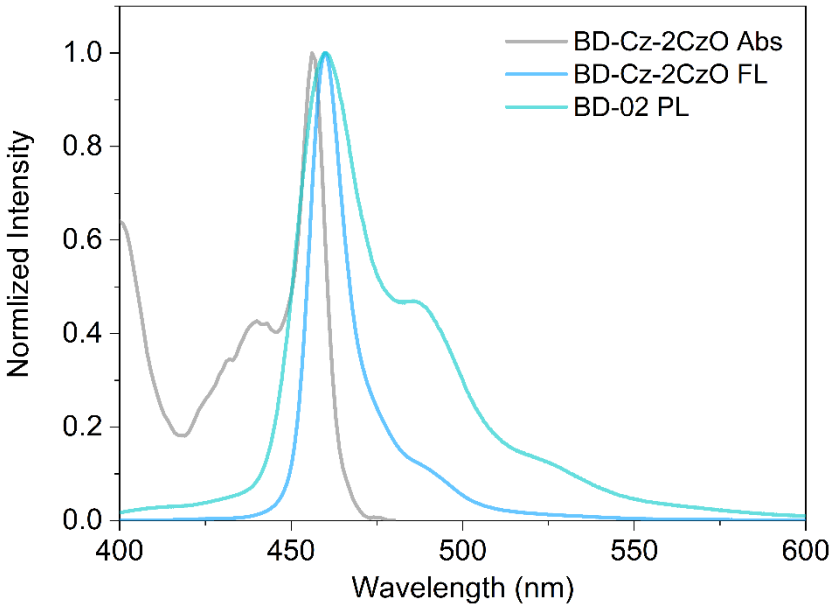

Supplementary Fig. 13 UV-vis absorption, emission spectra of BD-Cz-2CzO, and emission spectra of BD-02 in dilute toluene solution.

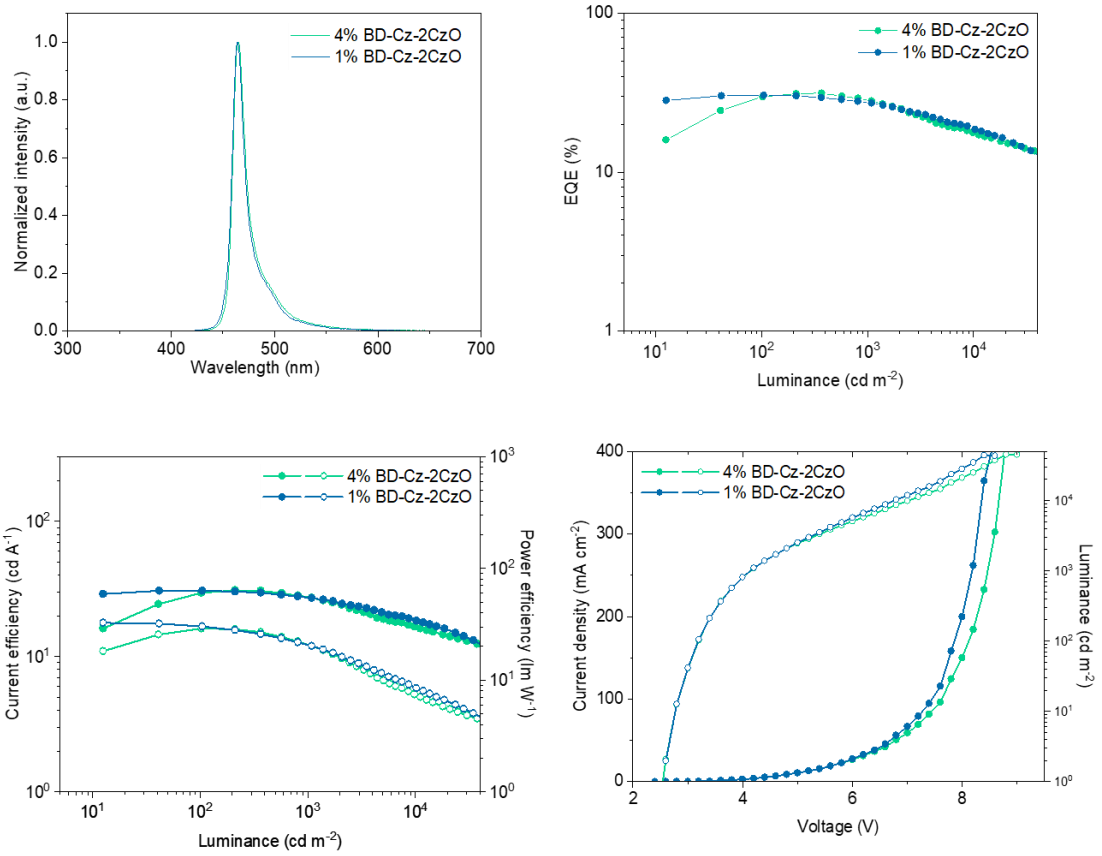

Supplementary Fig. 14 EL characteristics of devices based on BD-Cz-2CzO : EL spectra (recorded at 1000 cd m^{-2}) (a), external quantum efficiency -luminance (EQE-L) curves (b), Current and power efficiency-luminance (CE–L–PE) curves (c), and Current density-luminance-voltage (J–V–L) (d) at different doping ratios.

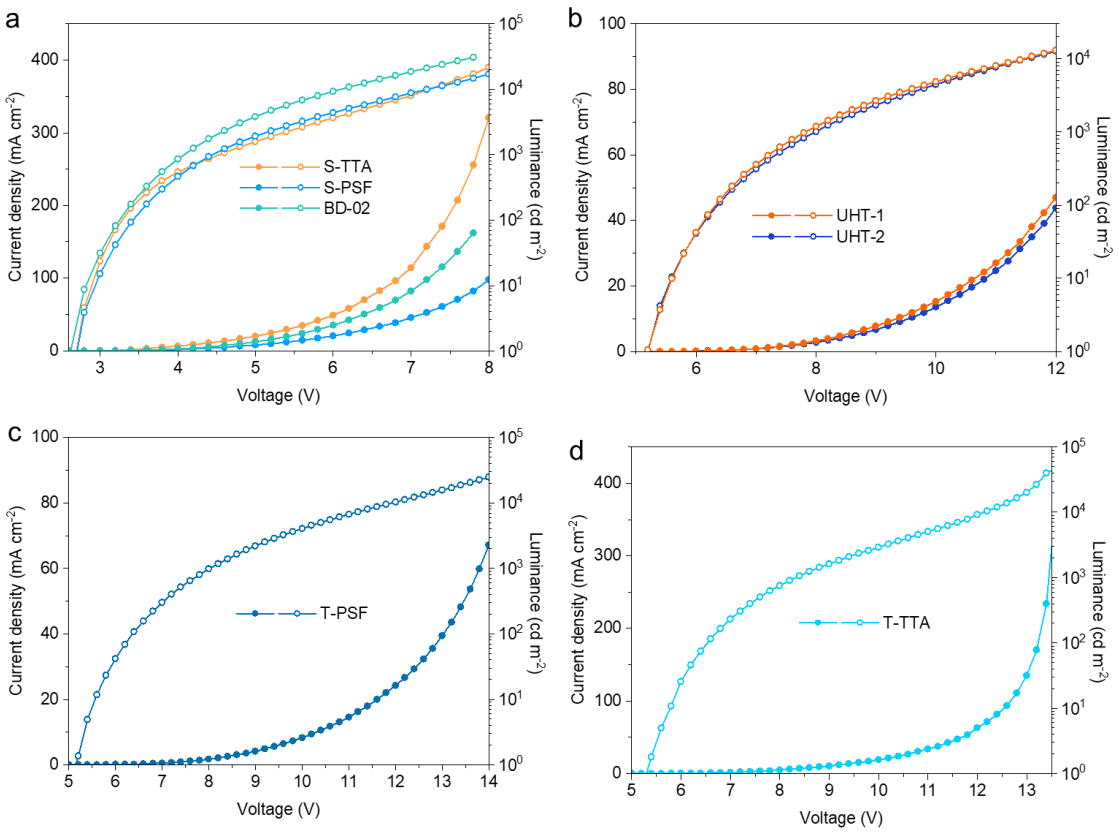

Supplementary Fig. 15 J-V-L characteristics of the single and tandem devices based on BD-Cz-2CzO. (a) J-V-L curves of S-TTA, S-PSF devices and reference device based on BD-02. (b) J-V-L curves of UHT-1 and UHT-2 devices. (c) J-V-L curves of T-PSF device. (d) J-V-L curves of T- TTA device.

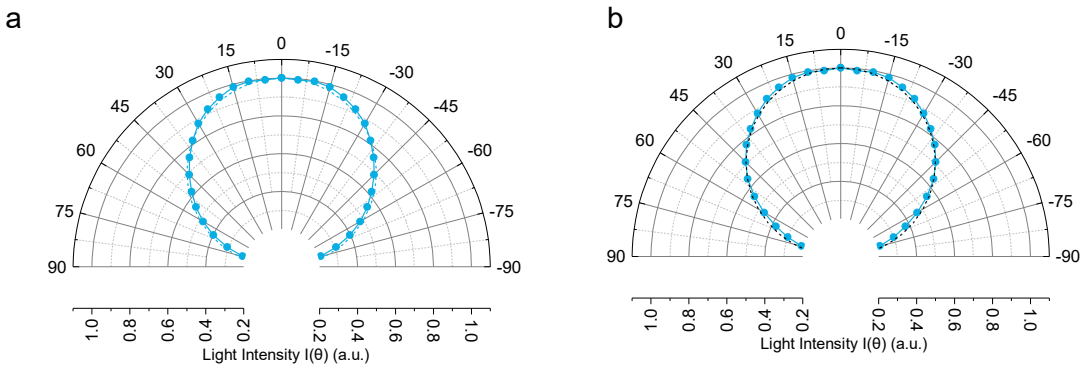

Supplementary Fig. 16 Angle-dependent EL intensities of (a) UHT-1 and (b) UHT-2 devices, compared to the Lambertian distribution.

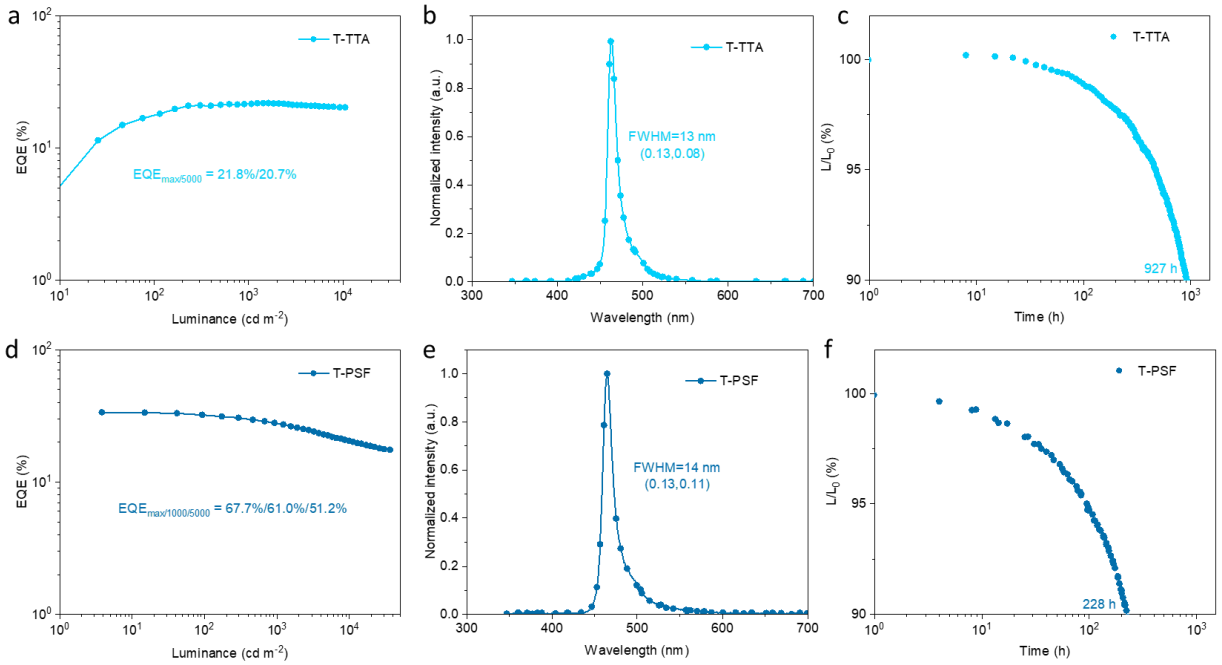

Supplementary Fig. 17 EL performance of the dual-unit tandem device with two TTA units (T-TTA) and two PSF units (T-PSF). (a,d) EQE-L curve. (b,e) EL spectra. (c,f) The operation lifetime of the devices at an initial luminance of 1,000 cd m^{-2}.

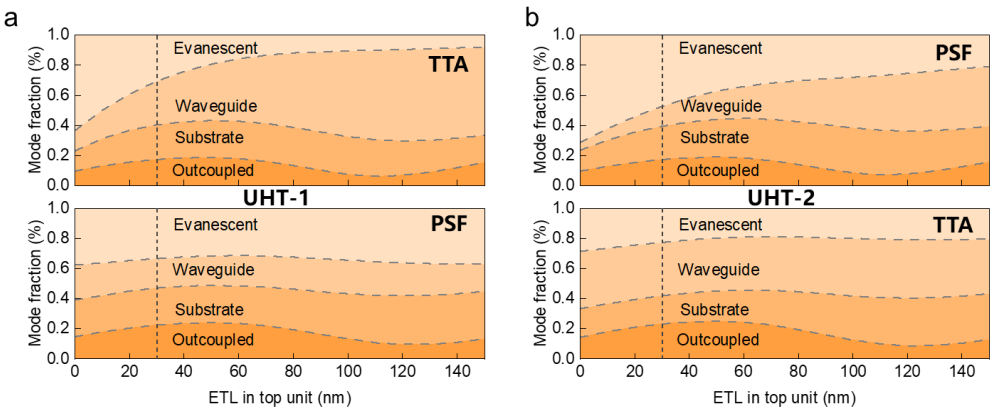

Supplementary Fig. 18 Optical simulation results of hybrid tandem OLED devices. Optical simulation results of the distribution of various optical modes of UHT-1 (a) and UHT-2(b).

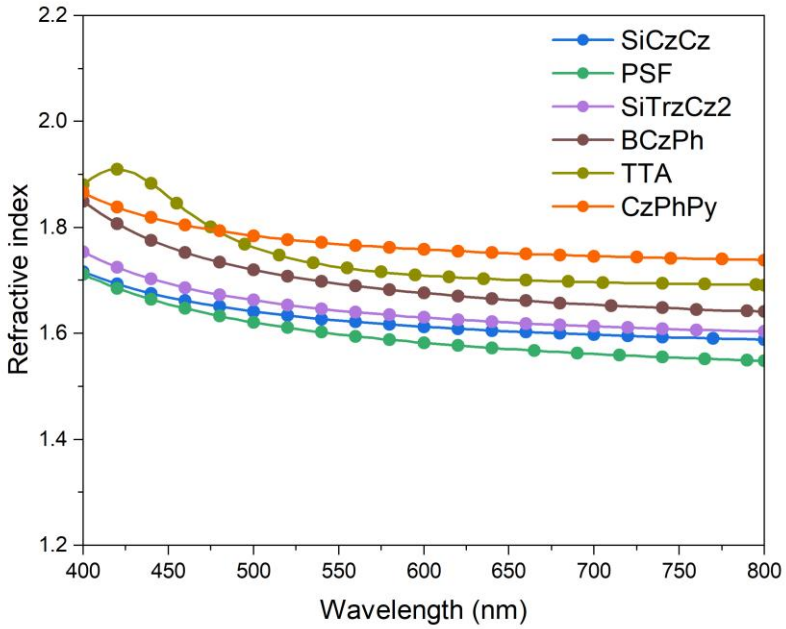

Supplementary Fig. 19 Refractive indexes of the charge blocking layers and EMLs in PSF-unit and TTA-unit.

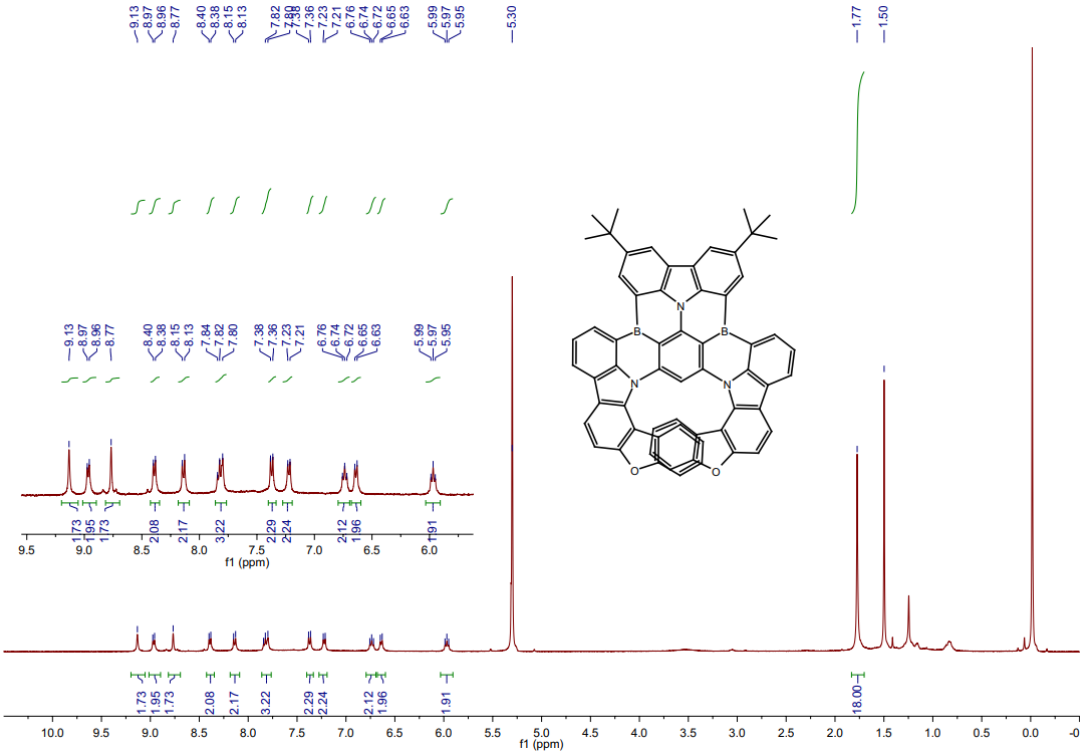

Supplementary Fig. 19 ^{1}H NMR spectrum of BD-Cz-2CzO in CD_2Cl_2.

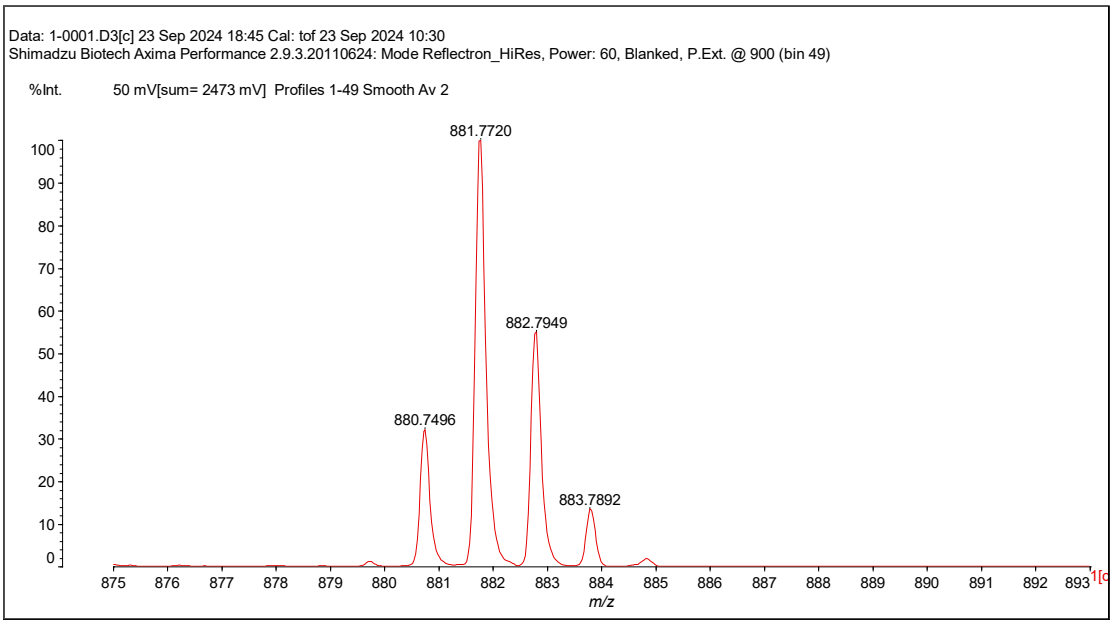

Supplementary Fig. 20 MALDI-TOF mass spectrum of BD-Cz-2CzO.

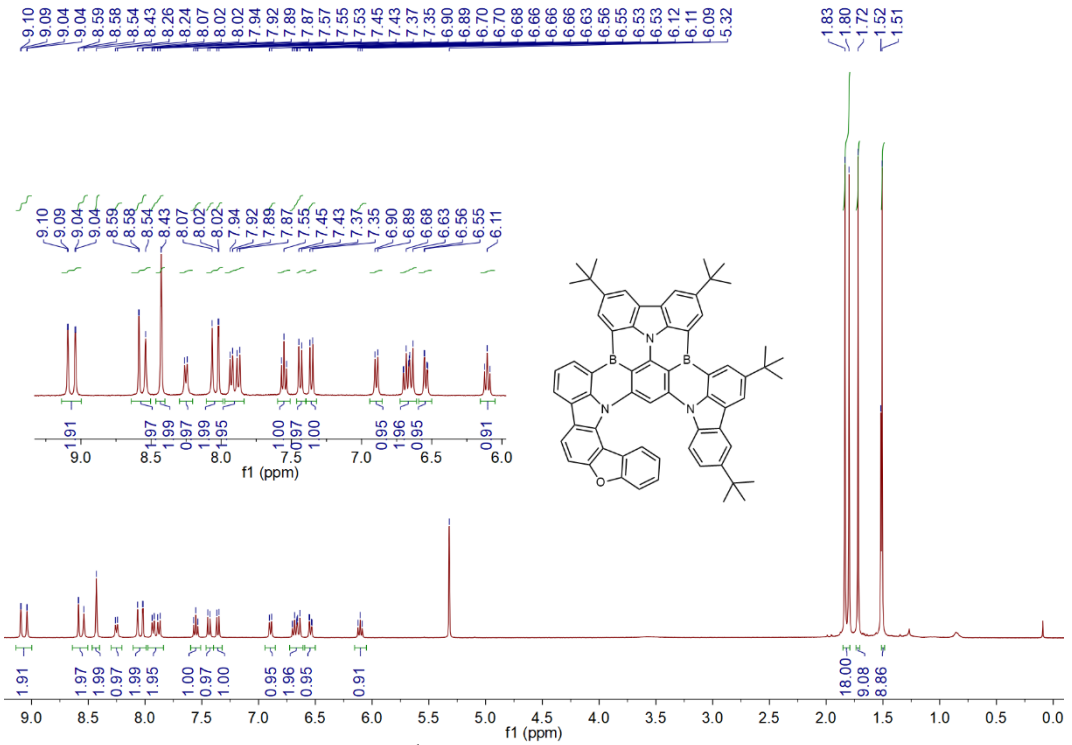

Supplementary Fig. 21 ^{1}H NMR spectrum of BD-2Cz-CzO in CD_2Cl_2.

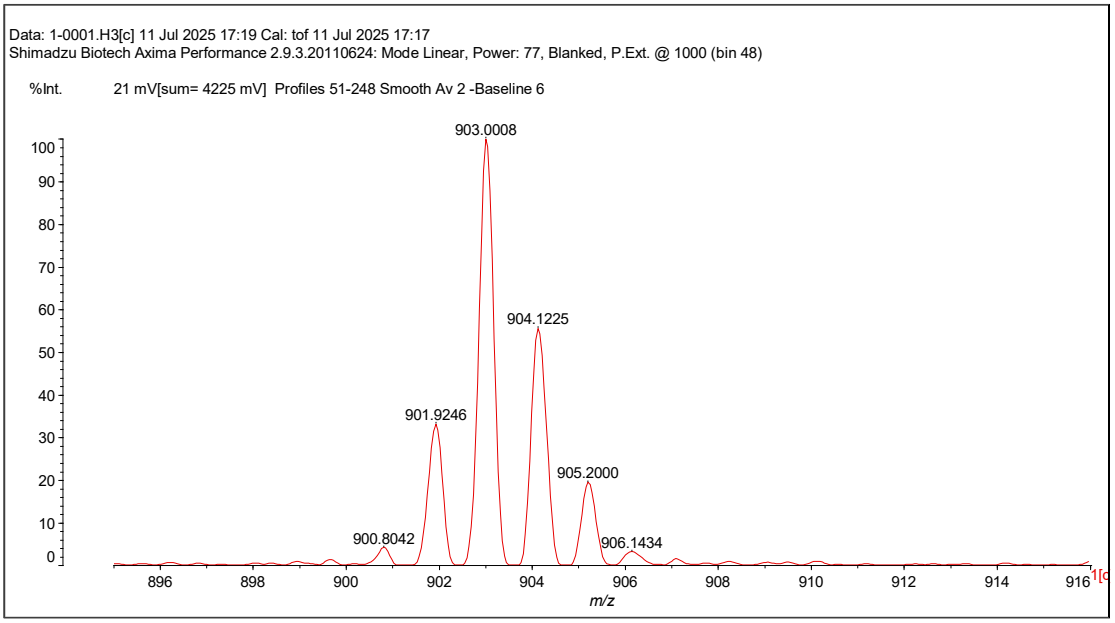

Supplementary Fig. 22 MALDI-TOF mass spectrum of BD-2Cz-CzO.

Supplementary Table 1. Summary of OLED performance employing deep-blue MR-TADF emitter .

Emitter	λ_{PL} (nm)	$FWHM_{PL}$ (nm)	λ_{EL} (nm)	$FWHM_{EL}$ (nm)	EQE_{max} (%)	CIE (x, y)	Ref.
BD-Cz-2CzO	460	12	464	14	33.5	(0.13, 0.11)	This work
BD-2Cz-CzO	466	14	466	18	31.3	(0.13, 0.12)	This work
[B-N]N2	438	16	441	20	20.3	(0.152, 0.046)	Adv. Mater. 2024, 36, 2409706.
ν-DABNA	468	14	469	18	34.4	(0.12,0.11)	Nat. Photon. 2019, 13, 678–682
BOBO-Z	441	15	445	18	13.6	(0.15,0.04)	Adv. Mater. 2022, 34, 2107951
V-DABNA-F	467	13	468	15	26.6	(0.12,0.10)	Adv. Sci. 2023, 10, 2205070
DOBN	438	19	449	20	35.4	(0.15, 0.04)	ACS Mater. Lett. 2024, 6, 3246−3253
m-ν-DABNA	464	14	471	18	36.2	(0.12, 0.12)	Chem. Eng. J. 2022, 432 134381
4F-ν-DABNA	457	14	464	18	35.8	(0.13,0.08)	Chem. Eng. J. 2022, 432 134381
4F-m-ν-DABNA	455	14	461	18	33.7	(0.13,0.06)	Chem. Eng. J. 2022, 432 134381
DBCz-Mes	452	14	452	17	33.9	(0.14, 0.06)	Sci. Adv. 2023, 9, eadh1434
DPA-B3	448	14	450	15	37.7	(0.15, 0.04)	Nat. Photon. 2024, 18, 1161–1169
DPA-B4	458	12	457	14	39.2	(0.14, 0.05)	Nat. Photon. 2024, 18, 1161–1169
ν-DABNA-Az1	453	14	459	19	30.8	(0.14, 0.08)	Adv. Mater. 2024, 36, 2402905
ν-DABNA-Az2	-	-	458	17	29.9	(0.14, 0.06)	Adv. Mater. 2024, 36, 2402905

ν-DABNA-Az3	-	-	459	20	33	(0.14, 0.10)	Adv. Mater. 2024, 36, 2402905
tBisICz-PhCz	440	16	446	19	24.9	(0.16, 0.04)	Adv. Sci. 2023, 10, 2302619
Cz-DICz	457	14	460	18	25.6	(0.14,0.10)	Adv. Sci. 2023, 10, 2302619
tBO-4B	449	13	452	16	30.3	(0.16, 0.04)	Adv. Mater. 2025, 37, 2500010.
pNAICZ-tPh	456	15	458	19	34.3	(0.15, 0.11)	Adv. Mater. 2025, 37, 2503839.
BN3	456	17	456	18	38.9	(0.14, 0.06)	Adv. Mater. 2025, 37, 2502459.
DBDS	452	16	456	18	39.6	(0.14, 0.06)	Adv. Mater. 2025, 37, 2502459.
DBDSe	453	17	456	18	40.5	(0.14, 0.06)	Adv. Mater. 2025, 37, 2502459.
3B-DPA	437	13	438	15	29.3	(0.15, 0.03)	Angew. Chem. Int. Ed. 2025, 64, e202503320.
Cz-DABNA	465	12	472	16	23.8	(0.14, 0.19)	Angew. Chem. Int. Ed. 2023, 62, e202313084.
t-BuCz-DABNA	466	12	472	16	29.2	(0.14, 0.19)	Angew. Chem. Int. Ed. 2023, 62, e202313084.

Supplementary Table 2. X-ray crystallographic data of BD-Cz-2CzO.

Temperature/K	193	Crystal system	monoclinic
Empirical formula	$C_{62}H_{41}B_2N_3O_2$	Formula weight	881.6
Space group	P2/c	Wavelength/ Å	1.34139
a/Å	10.7345(13)	α/°	90
b/Å	13.9793(16)	β/°	96.923(5)
c/Å	32.376(4)	γ/°	90
V/Å^3	4823.0(10)	Z	4
Dx/g cm^{-3}	1.214	μ/mm^{-1}	0.360
F(000)	1840.0	Reflections collected	22102
Independent reflections	8777	R(int)	0.1261
Data/restraints/parameters	8777/0/629	GOF on F^2	1.011
Final R indexes [$I \geq 2\sigma(I)$]	$R_1 = 0.0755$ $wR_2 = 0.1879$	R indexes (all data)	$R_1 = 0.1572$ $wR_2 = 0.2300$

Supplementary Table 3. X-ray crystallographic data of BD-2Cz-CzO.

Temperature/K	193	Crystal system	monoclinic
Empirical formula	$C_{64}H_{55}B_2N_3O$	Formula weight	903.7
Space group	C2/c	Wavelength/ Å	1.54178
a/Å	36.624(2)	α/°	90
b/Å	16.4197(10)	β/°	124.187(3)
c/Å	22.1087(15)	γ/°	90
V/Å^3	10997.9(13)	Z	8
Dx/g cm^{-3}	1.092	μ/mm^{-1}	0.487
F (000)	3824.0	Reflections collected	54488
Independent reflections	10118	R(int)	0.0876
Data/restraints/parameters	8777/0/629	GOF on F^2	1.111
Final R indexes [$I \geq 2\sigma(I)$]	$R_1 = 0.0991$ $wR_2 = 0.2804$	R indexes (all data)	$R_1 = 0.1311$ $wR_2 = 0.3200$

Supplementary Table 4 Summary of the photophysical properties of BD-3Cz, BD-2Cz-CzO, and BD-Cz-2CzO doped films.

Emitter	λ_{em}[a] (nm)	FWHM (nm)	Φ_{PL}[b] (%)	τ_p[c] (ns)	τ_d[c] (μs)	k_r[d] ($\times 10^8$ s^{-1})	k_{RISC}[e] ($\times 10^4$ s^{-1})
BD-3Cz	471	24	93	12	45	0.64	2.0
BD-2Cz-CzO	468	18	96	9	47	0.86	2.2
BD-Cz-2CzO	466	14	98	9	52	0.84	2.3

[a] Maximum emisssion peak [b] Absolute PL quantum yield evaluated using an integration sphere. [c] Emission lifetime of prompt fluorescence (τ_p) and delayed fluorescence (τ_d). [d] Rate constant of fluorescence radiative decay (S_1-S_0). [e] Rate constant of RISC (T_1-S_1).

Supplementary Table 5. Summary of the single-unit PSF devices based on BD-Cz-2CzO performances.

x wt%	λ_{EL}[a] (nm)	FWHM (nm)	EQE[b]$_{max/1000/5000}$ (%)	PE[c]$_{max/1000/5000}$ (lm W^{-1})	CE[d]$_{max/1000/5000}$ (cd A^{-1})	CIE[e] (x,y)
1%	464	14	30.3/27.1/21.4	32.5/20.3/11.5	30.7/27.1/21.3	(0.13,0.11)
2%	464	14	33.5/27.9/22.5	33.2/18.4/10.4	31.7/25.8/20.6	(0.13,0.11)
4%	464	14	31.3/28.0/19.9	29.0/20.3/9.9	30.8/27.1/18.9	(0.13,0.11)

[a] EL peak wavelength. [b] Maximum external quantum efficiency (EQE) and EQE at 1000 and 5000 cd m^{-2}. [c] Maximum power efficiency (PE) and PE at 1000 and 5000 cd m^{-2}. [d] Maximum current efficiency (CE) and CE at 1000 and 5000 cd m^{-2}. [e] CIE coordinates.

Supplementary Table 6. Summary of recent reported the-state-of-art stable bottom-emitting blue OLEDs with λ_{EL} ⩽467 nm.

Device	λ_{EL} (nm)	FWHM (nm)	$EQE_{max/1000}$ (%)	LT90 (h)	CIE_y	Ref.
S-PSF	464	14	33.5/27.9	150	0.11	This work
UHT1	464	14	46.3/42.4	263	0.11	This work
UHT2	464	14	39.7/37.2	539	0.10	This work
p4TCzPhBN	461	29	32.5/~25	25	0.12	Adv. Mater. 2020, 32, 1908355
BD-02	462	43	25.4/23.4	350	0.20	Nat. Photon. 2022, 16, 212–218
BD-02 (PSF)	~463	~37	~29/25.8	~200	0.165	Sci. Adv. 2022, 8, eabq1641
BD-02 (Tandem)	461	24	36.8/-	238	0.12	Nat. Photon. 2025,19, 607–614
Pt-SPCz	~460	22	25.1/21.1	60	0.13	Adv. Mater. 2024, 36, 2409394
Pt-SPCz (PSF)	460	26	28.1/25.3	40	0.096	Adv. Mater. 2024, 36, 2409394
Pt-SPCz (Tandem)	460	26	50.3/44.4	180	0.14	Adv. Mater. 2024, 36, 2409394
ν-DABNA-Az1	459	19	30.8/19.9	0.45	0.083	Adv. Mater. 2024, 36, 2402905
ν-DABNA-Az2	458	17	29.9/16	0.53	0.06	Adv. Mater. 2024, 36, 2402905
ν-DABNA-Az3	459	20	33.0/22.4	1.07	0.10	Adv. Mater. 2024, 36, 2402905
Ir(cb)3	462	-	14.4/-	31	0.17	Chem. Eng. J. 2022, 448, 137671
Pt-AdaPh	~461	-	22.6/-	0.05	0.12	Adv. Funct. Mater. 2021, 31, 2100967
Pt-dipCz	461	22	25/22.8	>20	0.16	Small Methods 2024, 8, 2301710
3B-DPA (HF)	438	15	29.3/-	~0.5 h	0.06	Angew. Chem. Int. Ed. 2025, 64, e202503320
pNAICZ-tPh (TSF)	458	19	34.3/26.9	40	0.11	Adv. Mater. 2025, 37, 2503839

5Cz-BNO (TSF)	462	31	36.3/21.4	~90	0.11	Angew. Chem. Int. Ed. 2025, 64, e202420489
PtON5-dtb	464	34	19.3/17.3	48	0.16	Adv. Funct. Mater. 2024, 34, 2405066
PtQS1	464	17	28.0/26.6	~20	0.11	Nat. Photon. 2025. doi.org/10.1038/s41566-025-01706-0
PtR2	466	22	29.2/27.3	~25	0.15	Nat. Photon. 2025. doi.org/10.1038/s41566-025-01706-0
Pt-Me-impy	466	27	22.8/20.3	~400	0.18	Adv. Mater. 2025. e10070.

Supplementary Table 7. Summarized EL performance of tandem TTA and PSF devices based on BD-Cz-2CzO

Device	λ_{EL} (nm)	FWHM (nm)	EQE_{max}/5000/10000 (%)	PE_{max}/5000/10000 (lm W^{-1})	CE_{max}/5000/10000 (cd A^{-1})	CIE (x,y)	LT90 (h)
T-PSF	464	14	67.7/61.0/51.2	35.2/22.7/14.5	65.1/57.7/47.8	(0.13,0.11)	228
T-TTA	463	13	21.8/20.7/20.2	6.8/4.3/3.8	15.7/15.0/14.7	(0.13,0.08)	927

[a] EL peak wavelength. [b] Maximum external quantum efficiency (EQE) and EQE at 5000 and 10000 cd m^{-2}. [c] Maximum power efficiency (PE) and PE at 5000 and 10000 cd m^{-2}. [d] Maximum current efficiency (CE) and CE at 5000 and 10000 cd m^{-2}. [e] CIE coordinates. [f] Recorded at an initial luminance of 1,000 cd m^{-2}.

References

1 Lukosz, W. Theory of optical-environment-dependent spontaneous-emission rates for emitters in thin layers. *Phys. Rev. B* **22**, 3030-3038 (1980).

2 Wasey, J. & Barnes, W. Efficiency of spontaneous emission from planar microcavities. *Journal of Modern Optics* **47**, 725-741 (2000).

3 Neyts, K. A. Simulation of light emission from thin-film microcavities. *J. Opt. Soc. Am. A* **15**, 962-971 (1998).

4 Furno, M., Meerheim, R., Hofmann, S., Lüssem, B. & Leo, K. Efficiency and rate of spontaneous emission in organic electroluminescent devices. *Phys. Rev. B* **85**, 115205 (2012).

5 Kim, J., Kang, K., Kim, K.-Y. & Kim, J. Origin of a sharp spectral peak near the critical angle in the spectral power density profile of top-emitting organic light-emitting diodes. *Jpn. J. Appl. Phys.* **57**, 012101 (2018).

6 Kang, K., Kim, K.-Y. & Kim, J. Theoretical comparison of the excitation efficiency of waveguide and surface plasmon modes between quantum-mechanical and electromagnetic optical models of organic light-emitting diodes. *Opt. Express* **26**, A955-A973 (2018).

7 Kim, J. & Kim, J. Theoretical Modeling and Analysis of the Contribution of the Near-Field Absorption to the Dipole Radiation Power in Top-Emitting Organic Light-Emitting Diodes. *Appl. Sci.* **11**, 3181 (2021).

8 Byrnes, S. Multilayer optical calculations. (2016). DOI: 10.48550/arXiv.1603.02720.